Protein J (2012) 31:425–431
DOI 10.1007/s10930-012-9419-4

Exploring the Energy Profile of Human IgG/Rat Anti-human IgG Interactions by Dynamic Force Spectroscopy

Zhengjian Lv · Jianhua Wang · Guoping Chen

Published online: 16 May 2012

Abstract Interactions between antibody and antigen molecules play essential roles in biological recognition processes as well as medical diagnosis. Therefore, an understanding of the underlying mechanism of antibody–antigen interactions at the single molecular level would be beneficial. In the present study, human immunoglobulin (IgG) tethered cantilevers and rat anti-human IgG functionalized gold surfaces were fabricated by using self-assembled monolayers method. Dynamic force spectroscopy was employed to characterize the interactions between human (IgG) and rat anti-human IgG at the single-molecule level. The unbinding forces were determined to be 44.6 ± 0.8, 65.8 ± 3.0, 108.1 ± 4.1, 131.1 ± 11.2, 149.5 ± 4.7, 239.5 ± 3.1 and 294.7 ± 7.7 pN with ramping loading rates of 514, 1,127, 3,058, 7,215, 15,286, 31,974 and 50,468 pN s^{-1}, respectively. In addition, the unbinding forces were found to be increasing with the logarithm of apparent loading rates in a linear way. Fitting data group resulted in two distinct linear parts, suggesting there are two energy barriers. The corresponding distances in the bound and transition states (x_β) and the dissociation rates (K_{off}) were calculated to be 0.129 ± 0.006 nm, 3.986 ± 0.162 s^{-1} for the outer barrier and 0.034 ± 0.001 nm, 36.754 ± 0.084 s^{-1} for the inner barrier. Such findings hold promise of screening novel drugs and discerning different unbinding modes of biological molecules.

Z. Lv · J. Wang (✉) · G. Chen
Key Laboratory of Biorheological Science and Technology, Ministry of Education, and Institute of Biochemistry and Biophysics, College of Bioengineering, Chongqing University, Chongqing 400044, China
e-mail: cqubio@hotmail.com

Keywords Human immunoglobulin · Rat anti-human IgG · Dynamic force microscopy · Energy profile

Abbreviations

AFM	Atomic force microscopy
DFS	Dynamic force spectroscopy
IgG	Immunoglobulin
MHA	16-Mercaptohexadecanoic acid
NHS	*N*-hydroxysulfosuccinimide
PPIs	Protein–protein interactions
SAMs	Self-assembled monolayers

1 Introduction

Interactions between antibody and antigen molecules play pivotal roles in drug design, medical diagnosis, immunoassay, biophysical research, molecular biology, etc. [21, 26, 27, 38, 45, 47]. The last decade had witnessed compelling achievements of protein–protein interactions (PPIs) related researches owing to the invention of scanning probe microscopy. These pioneering works are mostly regarding to either the single molecule imaging or the single molecule interacting forces. However, the interaction kinetics, bond association and dissociation of PPIs remain unclear. Some intriguing issues, like how long does a PPIs' bond survive? How strong is a single bond? How many energy barriers are required to be overcome to break the bound state and what is the energy profile along the separation pathway of a pair of interacting PPIs, etc. are not fully understood. Recent years, based on single molecule force spectroscopy, a force spectroscopy named dynamic force spectroscopy (DFS) has emerged with the power of recording a number of force data over broad loading rates.

The DFS possesses some advantages over other ensemble methods [10, 34] in ultra-sensitive force response, working at physiological conditions, reliable single molecule force measurements, enabling it becomes a powerful tool for probing PPIs. In such context, increasing interest has been aroused to this new inner world of PPIs, i.e. the dissociation kinetics and energy profile of an interacting PPIs.

It is well known that the measured unbinding forces are not intrinsic character of an interacting PPIs but depend on the apparent loading rates that are exerted on the complex [13, 14]. With ramping loading rates, the unbinding forces increase due to a linear relationship of unbinding forces on apparent loading rates. As soon as the DFS theory was introduced [12, 17], it was applied to explore some interactions between molecules of biological interests, such as β-casein/proteasome [11], ExpR protein/DNA fragment [1], digoxigenin/antibody [32], chaperonin GroEL/porcine pesin [37], fibrinogen/erythrocyte [9], LexA protein/DNA [25], P-selectin/P-selectin glycoprotein ligand-1 [20], P-selectin/ligand [18], sendai/anti-sendai antibody [22], and complementary DNA strands [39]. Despite this, little is known to the antibody based PPIs with DFS force measurements.

In this work, we chose human IgG and its antibody as a model interacting pattern. By performing DFS force measurements between these two molecules, we expected to explore the energy profile of characteristic interactions between human IgG and its antibody. This study could provide new insight into the antibody–antigen interactions at nanoscale level.

2 Materials and Methods

A prerequisite for running DFS with a pair of antigen–antibody is immobilizing either antigen or antibody molecules onto the surface of substrates whereas tethering the counterparts with AFM tips. To achieve this goal, an effective and efficient method called thiol-based SAMs was adopted for protein immobilization [16, 28]. The details of sample preparation, DFS measurements as well as data analysis are described as follows.

3 Materials

N-hydroxysulfosuccinimide (NHS), 1-ethyl-3-(dimethylaminopropyl) carbodiimide hydrochloride (EDC), and 16-mercaptohexadecanoic acid (MHA) were procured from Sigma Aldrich Chemical Co. and used without further purification. Ethanol (guaranteed grade) and phosphate buffered saline (PBS, 140 mM NaCl, 3 mM KCl, pH 7.4) were purchased from Merck Co. MilliQ water (of 18.2 MΩ cm resistivity) was obtained by purifying through Millipore system. Human IgG and its antibody rat anti-human IgG were purchased from Biosun Co.

3.1 Gold-Covered Mica Substrates

Gold-covered mica substrates were fabricated by vapor deposition method, of which gold was sputtered onto freshly cleaved mica surfaces in an evaporator. The rates of evaporation were set at 0.1–0.3 nm/s, and the final height of gold layers was <200 nm [27]. There is a chromium film which locates between the gold layer and mica surface to strength the connection of these surfaces. The gold-covered mica surfaces were then annealed in H_2 flame for 1 min prior to any use.

3.2 SAMs Chemistry for Substrates and AFM Tips

The surface chemistry for substrates and AFM tips was performed as shown in previously published literature [29], and the procedures are listed below. The gold-covered mica substrates fabricated as abovementioned were entirely cleaned in a freshly prepared piranha solution (v/v H_2SO_4:H_2O_2 = 3:1) for 30 min. The step of cleaning was conducted with extreme caution as piranha solution is very sensitive to organic chemicals. The substrates were then sunk into an ethanol solution (100 % v/v) of 1 milli-molar MHA for 24 h to generate thiols films supported by gold surfaces, and unreacted thiols were washed away by ultrasonicating in pure ethanol for 2 min. The obtained thiols films were then rinsed copiously with absolute ethanol, MilliQ water, and finally dried with a nitrogen flow. Further protein immobilization onto the thiols films was conducted as described before with minor changes [44]. Briefly, the thiol films were immersed into a solution of NHS (2 mg/ml) and EDC (2 mg/ml) in PBS buffer solution for 1 h, of which the carboxylic acid groups were activated. After thoroughly rinsed with MilliQ water, and dried with a nitrogen flow, the active thiols films were then nurtured with an antibody solution with concentration of 7 μg/ml and allowed for incubating at 4° for 8 h to link the protein molecules onto the thiols films. The obtained samples of protein SAMs were kept under four degrees before use. The same protocol was applied to functionalize the AFM tips with human IgG except the final incubation time was shortened to 6 h.

3.3 DFS Force Measurements

DFS between human IgG and its antibody was recorded by a scanning probe microscope with a model of CSPM 5000 (Benyuan Co., China). AFM cantilevers (SiNi, Budget-Sensors) with nominal spring constants of ~60 pN/nm

were used. By varying the retract velocity, a series of apparent loading rates ranged from 514 to 50,468 pN/s were set for DFS force measurements. At each particular retract velocity, the force measurements between antigen and antibody were recorded over some small areas (5 × 5 μm in size) onto the antibody surface to obtain a sufficient sample size for further data analysis.

3.4 Data Analysis

The unbinding forces against the logarithm of apparent loading rates can be plotted. An equation based on the Bell-Evans model can be used to extract the kinetic parameters [3, 15]:

$$F = \frac{k_B T}{x_\beta} \ln\left(\frac{r x_\beta}{k_{off} k_B T}\right) \quad (1)$$

where F (pN) is the unbinding force, k_B (J K^{-1}) is the Boltzman constant, T is the absolute temperature (K), r is the loading rate (pN s^{-1}), x_β is the distance between bound state and intermediate state (nm), which equals the slope of fitting curve, and k_{off} is the dissociation rate of bond at zero applied force (s^{-1}), which can be calculated with the intercept of fitting curve. Once k_{off} has been determined, the height of energy barrier, $\Delta G^{\#}$ can be deduced according to the following equation (kJ mol^{-1}):

$$k_{\text{off}} = \frac{k_B T}{h} \exp\left(\frac{-\Delta G^{\#}}{k_B T}\right) \quad (2)$$

where h is the Planck constant, $k_B T$ is the thermal energy. For all unbinding force histograms which were subjected to Gaussian fit, the bin width of each histogram was estimated by the following equation [36]:

$$h_n = 3.49 s n^{-1/3} \quad (3)$$

where h_n is the optimal bin width, s is the estimated standard deviation, n is the total counts.

4 Results and Discussion

4.1 Rationale of Single Molecule Force Spectroscopy

We took advantage of NHS exclusively covalently binding to the lysine group of protein molecules. This site-specific attachment ensures only a small amount of protein molecules would be sparsely immobilized onto the substrates and AFM tips, hence about one unbinding event out of ten pulling cycles will be recorded. According to the Poisson statistics, over 90 % of the detected unbinding events will be single unbinding events [42]. The MHA was chosen to circumvent the multidispersity of long linker, like poly ethylene (PEG), yet can be served as a short spacer to sort out the nonspecific interactions which often take place between tips and substrates with very short separation. Upon SMFS force measurements, the non-covalent interaction forces between antigen and antibody (usually lower than 500 pN) are much smaller than those covalent ones (larger than 1 nN) [4]. Therefore, during the force measurement with typical unbinding events, it is conceivable that the bond between antigen and antibody will dissociate preceding those covalent ones, justifying the unbinding event.

A scheme of the experimental setup is shown in Fig. 1a. The antigen functionalized AFM tip inspects over the well defined antibody monolayer. Upon one particular location, initially the tip is far away from the sample surface, there are no interactions at all such that the cantilever does not deflect. Then the tip is driven to move toward and suddenly jump onto the sample surface due to the attractive intermolecular force. The tip will keep pressing the sample to reach the trigger force and retracts after a short dwell. After that, the tip eventually jumps off the sample surface, resulting in a snap-off in the retraction curve, which can be recorded as "voltage–displacement" movements and translated into "force–distance" curves (Fig. 1b) [8]. To verify the specificity of detected interaction between human IgG and its antibody, a blocking experiment was also carried out on the corresponding surface by blocking the human IgG functionalized AFM tip with free antibody molecules. The resulting force–distance curve showed no interaction between blocked tip and antibody sample (Fig. 1c). Such finding corroborates the predicted specificity.

4.2 The Unbinding Force is Loading-Rate Dependent

It is widely acknowledged that the specific unbinding forces of antibody–antigen rely on the intrinsic interaction of molecules as well as on the apparent loading rates. By evaluating the unbinding forces at different apparent loading rates, the details of the dissociation dynamics of antibody–antigen and the barriers being traveled in the energy landscape through its dissociation coordinate can be inferred. In our case, the unbinding forces were also found to be linearly depended on the logarithm of apparent loading rates according the Eq. 1. As shown in Fig. 2a–g, the determined unbinding forces went up with increasing apparent loading rates. More specifically, the most probable unbinding forces were 44.6 ± 0.8, 65.8 ± 3.0, 108.1 ± 4.1, 131.1 ± 11.2, 149.5 ± 4.7, 239.5 ± 3.1 and 294.7 ± 7.7 pN with apparent loading rates of 514, 1,127, 3,058, 7,215, 15,286, 31,974 and 50,468 pN s^{-1}, respectively. The percentage of the frequency of unbinding events on each unbinding force histogram ranged from 6 to 13 %. The most probable unbinding forces were further plotted

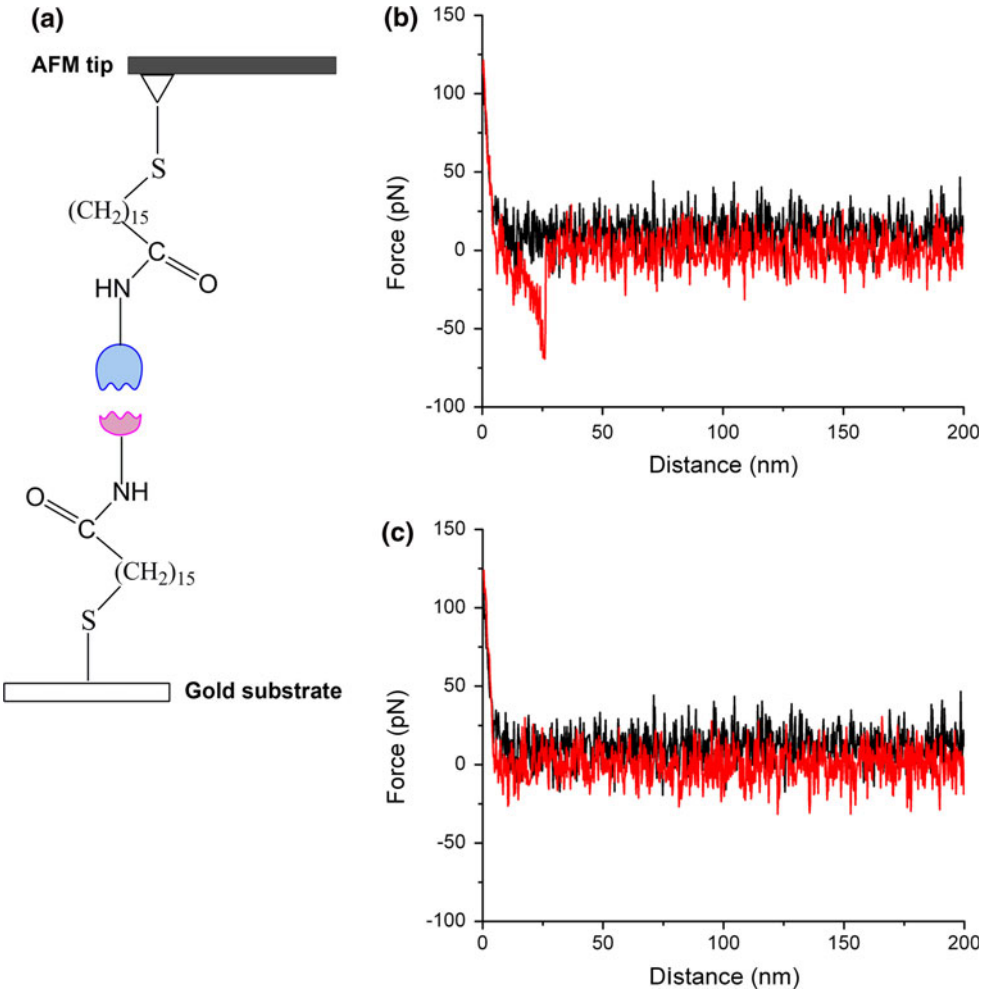

Fig. 1 A scheme of experimental setup (**a**). Rat anti-human IgG and human IgG were immobilized onto the gold substrates and the AFM tips by SAMs method using identical MHA thiols molecules. A typical force-distance curve of specific interactions of antigen–antibody (**b**) shows there is a peak at a distance of 25.8 nm, corresponding to an unbinding event, whereas a typical force-distance curve of a blocking experiment just shows the noise of the instrument, indicating there is no specific interactions (**c**). A background noise level of 23.8 ± 4.5 pN was introduced because of thermal and other stochastic noises [19]

against the logarithm of apparent loading rates (Fig. 3a). By fitting the data points with Eq. 1, two distinct linear parts were observed. It yielded 0.129 ± 0.006 nm and 0.034 ± 0.001 nm for $x_{\beta 1}$ and $x_{\beta 2}$ plus 3.986 ± 0.162 s^{-1} and 36.754 ± 0.084 s^{-1} for K_{off1} and K_{off2}, respectively. These results implicate that there are two energy barriers existing in the energy landscape (Fig. 3b), of which the outer (low loading regime) and inner barrier (high loading regime) have an energy of 28.07 k_BT and 25.85 k_BT, respectively. Comparisons between the present study and literature reports were summarized in Table 1. The heights of present energy barriers were close to those of misfolded amyloid peptides [23], but stronger than those of Tax-interacting protein-1 (TIP-1)/TIP-1's recognition peptide (PDZ-pep) [30]. Moreover, the potential width x_β fell well into the energy range of typical ligand–receptor interactions like cytochrome C 551/azurin [6] and Human CD1D/alpha-galactosylceramide [7], to mention a few. This short potential width explicitly indicated a unique unbinding mechanism, of which there is a snap of bond other than a slow "unpeeling" or sliding of the antigen forward the antibody or vice verse. This kind of bond unbinding could be assigned to hydrogen bonds which take place at short distance other than van der Waals or hydrophobic interactions and be accounted for the specificity of detected interactions [25].

4.3 Energy Profile of Human IgG/Rat Anti-human IgG Interactions

The existence of two energy barriers in the interactions of human IgG and its antibody suggests the antigen binds to its antibody with avidity, which is a common phenomenon during the binding process of ligand–receptor interactions [5, 41], resulting in increased complexity in antibody–antigen systems. With avidity, antibody molecules are capable of binding to antigen molecules through either one or both paratopes [33]. In the framework of Bell-Evans model, the width of energy barrier is usually considered as a rough estimation of the steepness of the binding potential i.e. an estimation of the extent to which the formed interacting complex can be relaxed or deformed before it eventually falls apart [31]. In our case, the width of inner energy barrier is smaller than 1 Å, indicating the bonding

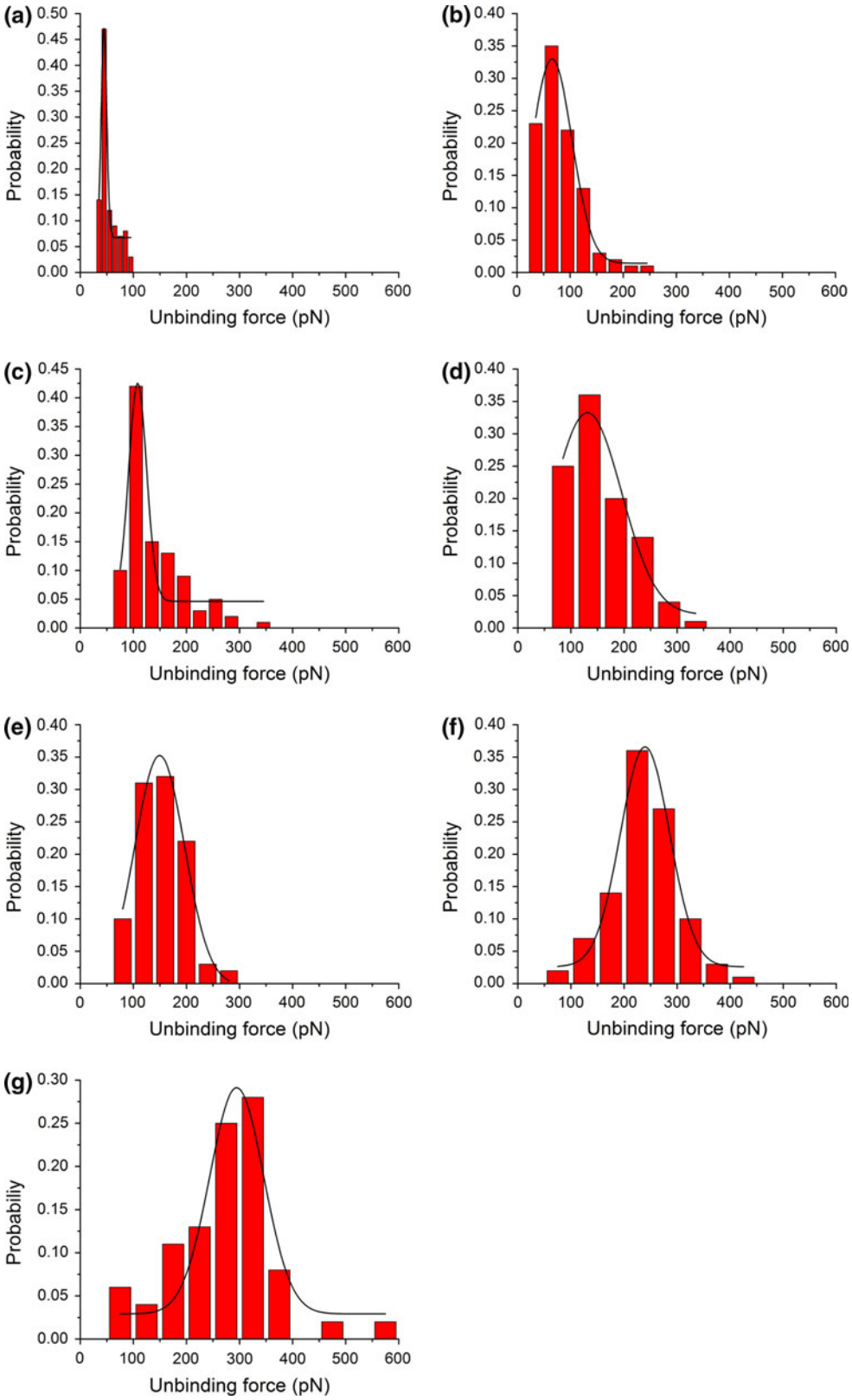

Fig. 2 Histograms of the determined unbinding forces between antibody and antigen. From **a** to **g** are the unbinding forces at apparent loading rates of 514, 1,127, 3,058, 7,215, 15,286, 31,974 and 50,468 pN s^{-1}, respectively. The most probable unbinding forces for **a**–**g** are 44.6 ± 0.8, 65.8 ± 3.0, 108.1 ± 4.1, 131.1 ± 11.2, 149.5 ± 4.7, 239.5 ± 3.1, 294.7 ± 7.7 pN, respectively. *Solid lines* are Gaussian fits. All Y axes are normalized probability. For each histogram, the data are collected by analyzing 100 force curves. The inconsistent force threshold for unbinding force histograms results from the discarding of some suspicious unbinding events

complex cannot withstand large deformation when a high force exerts. While for the outer barrier, the width is larger than 1 Å, implying the interacting complex is stabilized by strong contacts and goes through a great extent of stretching before it dissociates [43]. In addition, the depth of the energy barrier is associated with the affinity of

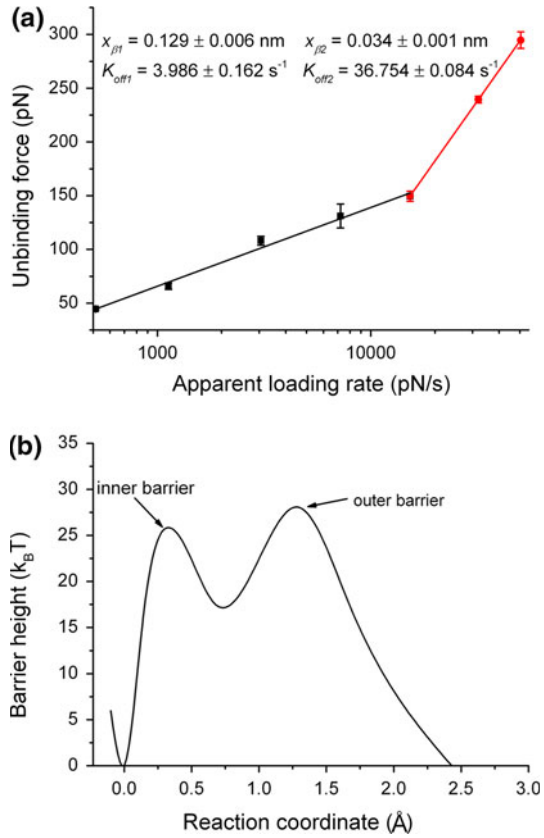

Fig. 3 Dynamic force spectra. **a** Fitting the data with Eq. 1 yields two distinct linear parts. Therefore, the positions of energy barriers together with the thermal energies are derived. For barrier 1 (outer barrier, colored in black) which is located in the outer space, the $x_{\beta 1}$ and the K_{off1} are calculated to be 0.129 ± 0.006 nm, K_{off1} = 3.986 ± 0.162 s^{-1}, respectively. For barrier 2 (inner barrier, colored in red) which lies in the inner space, the $x_{\beta 2}$ and K_{off2} are determined to be 0.034 ± 0.001 nm, 36.754 ± 0.084 s^{-1}, respectively. Some *error bars* are indistinguishable due to the relatively small SD values. In addition, a sketch of the energy landscape is shown Fig. 3b. (Color figure online)

antibody binding to antigen. The K_{off} of outer barrier is found to be 3.986 ± 0.162 s^{-1}, which is significantly lower than that of inner barrier (36.754 ± 0.084 s^{-1}), highlighting strong interactions between human IgG and its antibody when the interacting system is applied with a low external force.

The inverse of the dissociation rate of a bond gives the bond lifetime. In the present study, the bond lifetimes of the outer barrier and inner barrier are determined to be 0.25 and 0.027 s, respectively. These two distinct lifetimes, combined with the observed linear relationship of apparent loading rates against unbinding forces (Fig. 3), suggest the stability of the bond decreases with increasing applied force. Such response of a bond lifetime to the ramping of the applied force is reminiscent of other receptor–ligand system [24], indicating human IgG forms a slip bond with its antibody upon binding. One plausible contribution to the decline of bond lifetime upon rising applied force could be the rigidity of the human IgG molecule. When a high force is applied on the interacting system, the stability of bond diminishes with the increasing rigidity of the antigen.

5 Conclusions

The interactions of human IgG immobilized on the AFM tips and its antibody anchored on the gold surface have been successfully investigated by dynamic force spectroscopy. The unbinding forces between human IgG and its antibody were calculated to be 44.6 ± 0.8, 65.8 ± 3.0, 108.1 ± 4.1, 131.1 ± 11.2, 149.5 ± 4.7, 239.5 ± 3.1 and 294.7 ± 7.7 pN with apparent loading rates of 514, 1,127, 3,058, 7,215, 15,286, 31,974 and 50,468 pN s^{-1}, respectively. The dependence of unbinding forces on apparent

Table 1 Comparisons of energy profiles between the present study and literature reports

Pair	K_{off} (s^{-1})	x_β (nm)	k_BT	ΔG (kJ mol^{-1})
Human IgG/rat anti-human IgG [the present study]	K_{off1} = 3.986 ± 0.162	$x_{\beta 1}$ = 0.129 ± 0.006	28.07	
	K_{off2} = 36.754 ± 0.08	$x_{\beta 2}$ = 0.034 ± 0.001	25.85	
Alpha-synuclein/alpha-synuclein [35]	64 ± 7	0.10 ± 0.03	–	12 ± 3
Cytochrome C 551/azurin [6]	14 ± 2	0.14 ± 0.01	–	–
Apo-transferrin (Tf)/Tf receptor [46]	0.25 ± 0.08	8.1 ± 1.0	19	
Mucin1/mucin1 antibody [40]	2.6 × 10^{-3}	2.8 ± 0.2	6.5	
Glycoprotein Ib-IX/von willebrand Factor [2]	5.47 ± 0.25	0.71 ± 0.03	–	–
Tax-interacting protein-1 (TIP-1)/TIP-1's recognition peptide (PDZ-pep) [30]	K_{off1} = 1.10 × 10	$x_{\beta 1}$ = 0.04	5.14	
	K_{off2} = 2.77 × 10^{-2}	$x_{\beta 2}$ = 0.21	10.52	
Human CD1D/alpha-galactosylceramide [7]	1.94 ± 1.44	0.43 ± 0.10	–	–
Amyloid beta peptide 40/amyloid beta peptide 40 [23]	K_{off1} = 0.9 ± 0.2	$x_{\beta 1}$ = 0.265 ± 0.027	29.5	
	K_{off2} = 114 ± 12	$x_{\beta 2}$ = 0.028 ± 0.005	24.7	

loading rates was also investigated. The results suggested that the unbinding forces of human IgG and rat anti-human IgG increase linearly with the logarithm of the apparent loading rates. Furthermore, two energy barriers were reconstructed by deducing the transition distance and the thermal energy. The results provided novel insight for the unraveling of the specific interactions of antibody and antigen. This study has demonstrated the benefits of applying DFS on understanding the specific antibody–antigen interactions at the single molecule level. It could be extended in nanoprobing various antibody–antigen pairs and discovering the energy landscapes of dynamic recognition processes.

Acknowledgments This work was supported by the National Natural Science Foundation of China (No. 30670496, 30770529) and the Scientific Research Foundation for the Returned Overseas Chinese Scholars, State Education Ministry (2006-331) and the Natural Science Foundation Project of CQ CSTC (2006BB5017).

Conflict of interest The authors declare no conflict of interest.

References

1. Anselmetti D, Bartels FW, Becker A, Decker B, Eckel R, McIntosh M, Mattay J, Plattner P, Schafer C, Sewald N (2008) Langmuir 24:1365–1370
2. Arya M, Kolomeisky AB, Romo GM, Cruz MA, Lopez JA, Anvari B (2005) Biophys J 88:4391–4401
3. Bell GI (1978) Science 200:618–627
4. Beyer MK, Clausen-Schaumann H (2005) Chem Rev 105: 2921–2948
5. Bjornham O, Bugaytsova J, Boren T, Schedin S (2009) Biophys Chem 143:102–105
6. Bonanni B, Kamruzzahan ASM, Bizzarri AR, Rankl C, Gruber HJ, Hinterdorfer P (2005) Biophys J 89:2783–2791
7. Bozna BL, Polzella P, Rankl C, Zhu R, Salio M, Shepherd D, Duman M, Cerundolo V, Hinterdorfer P (2011) J Biol Chem 286:15973–15979
8. Cappella B, Dietler G (1999) Surf Sci Rep 34:1–104
9. Carvalho FA, Connell S, Miltenberger-Miltenyi G, Pereira SV, Tavares A, Ariens RAS, Santos NC (2010) ACS Nano 4: 4609–4620
10. Chaires JB (2008) Annu Rev Biophys 37:135–151
11. Classen M, Breuer S, Baumeister W, Guckenberger R, Witt S (2011) Biophys J 100:489–497
12. Evans E (1999) Faraday Discuss 111:1–16
13. Evans EA, Calderwood DA (2007) Science 316:1148–1153
14. Evans E, Leung A, Heinrich V, Zhu C (2004) Proc Natl Acad Sci USA 101:11281–11286
15. Evans E, Ritchie K (1999) Biophys J 76:2439–2447
16. Ferretti S, Paynter S, Russell DA, Sapsford KE, Richardson DJ (2000) Trends Analyt Chem 19:530–540
17. Merkel R, Nassoy P, Leung A, Ritchie K, Evans E (1999) Nature 397:50–53
18. Fritz J, Katopodis AG, Kolbinger F, Anselmetti D (1998) Proc Natl Acad Sci USA 95:12283–12288
19. Giessibl FJ (2003) Rev Mod Phys 75:949–983
20. Hanley W, McCarty O, Jadhav S, Tseng Y, Wirtz D, Konstantopoulos K (2003) J Biol Chem 278:10556–10561
21. Hinterdorfer P, Dufrene YF (2006) Nat Methods 3:347–355
22. Kienberger F, Kada G, Mueller H, Hinterdorfer P (2005) J Mol Biol 347:597–606
23. Kim BH, Palermo NY, Lovas S, Zaikova T, Keana JFW, Lyubchenko YL (2011) Biochemistry 50:5154–5162
24. Kim J, Zhang CZ, Zhang X, Springer TA (2010) Nature 466: 992–995
25. Kuhner F, Costa LT, Bisch PM, Thalhammer S, Heckl WM, Gaub HE (2004) Biophys J 87:2683–2690
26. Lee W, Oh BK, Min Bae Y, Paek SH., Hong Lee W, Choi JW (2002) Biosens Bioelectron 19: 185-192
27. Li L, Chen S, Oh S, Jiang S (2002) Anal Chem 74:6017–6022
28. Love JC, Estroff LA, Kriebel JK, Nuzzo RG, Whitesides GM (2005) Chem Rev 105:1103–1169
29. Lv Z, Wang J, Deng L, Chen G (2009) Nanoscale Res Lett 4: 1403–1408
30. Maki T, Kidoaki S, Usui K, Suzuki H, Ito M, Ito F, Hayashizaki Y, Matsuda T (2007) Langmuir 23:2668–2673
31. Morfill J, Blank K, Zahnd C, Luginbuhl B, Kuhner F, Gottschalk KE, Pluckthun A, Gaub HE (2007) Biophys J 93:3583–3590
32. Neuert G, Albrecht C, Pamir E, Gaub HE (2006) FEBS Lett 580:505–509
33. Odorico M, Teulon JM, Bessou T, Vidaud C, Bellanger L, Chen SW, Quemeneur E, Parot P, Pellequer JL (2007) Biophys J 93: 645–654
34. Pellecchia M, Bertini I, Cowburn D, Dalvit C, Giralt E, Jahnke W, James TL, Homans SW, Kessler H, Luchinat C, Meyer B, Oschkinat H, Peng J, Schwalbe H, Siegal G (2008) Nat Rev Drug Discov 7:738–745
35. Ray C, Akhremitchev BB (2005) J Am Chem Soc 127: 14739–14744
36. Scott DW (1979) Biometrika 66:605–610
37. Sekiguchi H, Arakawa H, Taguchi H, Ito T, Kokawa R, Ikai A (2003) Biophys J 85:484–490
38. Stroh C, Wang H, Bash R, Ashcroft B, Nelson J, Gruber H, Lohr D, Lindsay SM, Hinterdorfer P (2004) Proc Natl Acad Sci USA 101:12503–12507
39. Strunz T, Oroszlan K, Schafer R, Guntherodt H (1999) Proc Natl Acad Sci USA 96:11277–11282
40. Sulchek TA, Friddle RW, Langry K, Lau EY, Albrecht H, Ratto TV, DeNardo SJ, Colvin ME, Noy A (2005) Proc Natl Acad Sci USA 102:16638–16643
41. Sulchek T, Friddle R, Ratto T, Albrecht H, DeNardo S, Noy A (2009) Ann NY Acad Sci 1161:74–82
42. Tees DF, Waugh RE, Hammer DA (2001) Biophys J 80:668–682
43. Teulon JM, Parot P, Odorico M, Pellequer JL (2008) Biophys J 59:L63–L65
44. Wakayama J, Sekiguchi H, Akanuma S, Ohtani T, Sugiyama S (2008) Anal Biochem 380:51–58
45. Wojcikiewicz EP, Abdulreda MH, Zhang X, Moy VT (2006) Biomacromolecules 7:3188–3195
46. Yersin A, Osada T, Ikai A (2008) Biophys J 94:230–240
47. Zhu H, Bilgin M, Snyder M (2003) Annu Rev Biochem 72: 783–812